Inherent structure theory of liquids in the hard-sphere limit

Frank H. Stillinger and Thomas A. Weber
AT&T Bell Laboratories, Murray Hill, New Jersey 07974

(Received 4 June 1985; accepted 26 July 1985)

Atomic pair correlation functions for liquids provide an image of temperature-dependent short-range order. If the thermal ensemble of atomic configurations is mapped (by steepest descent on the potential hypersurface) onto potential energy minima, the pair correlation function from the resulting transformed configurations exhibits substantial image enhancement, revealing short-range order in a much more vivid fashion. Previous studies of model atomic liquids have demonstrated that at fixed density, mapped short-range order is virtually independent of the initial temperature, and thereby amounts to an "inherent structure" for the liquid. The present paper investigates steepest-descent mapping and inherent structure for hard spheres, construed as the infinite-n limit for pair potentials $(a/r)^n$. Methods used are both analytical and simulational, the latter involving molecular dynamics for $n = 12$ and 24. Results show that inherent structures in the hard-sphere limit are randomly packed configurations, where particle radii have been inflated to the point of jamming.

I. INTRODUCTION

Realistic models for interactions among particles in condensed phases require potential functions $\Phi(\mathbf{r}_1 \ldots \mathbf{r}_N)$ that are bounded from below, and are arbitrarily many times differentiable when all interparticle distances $r_{ij} > 0$. In attempting to understand both static structure as well as kinetic processes in such many body systems it is instructive to divide the $3N$-dimensional configuration space exhaustively into "basins," one surrounding each local minimum of Φ.[1-4] This division is accomplished by a mapping that connects any configuration $\mathbf{r}_1 \ldots \mathbf{r}_N$ to $\mathbf{r}_{1\alpha} \ldots \mathbf{r}_{N\alpha}$, a nearby configuration at which Φ is locally a minimum. The collection of all starting configurations which map onto a given minimum α defines the basin B_α for that minimum.

In the case of identical structureless spherical particles, the appropriate mapping is generated by the following steepest descent equations $(s \geqslant 0)$[1,3]:

$$d\mathbf{r}_j(s)/ds = -\nabla_j \Phi[\mathbf{r}_1(s) \ldots \mathbf{r}_N(s)]. \tag{1.1}$$

Starting from the given N-particle configuration as initial condition, the solution to Eq. (1.1) for positive s displaces the configuration along the direction of the negative of the potential gradient (in $3N$ dimensions) until it comes to rest $(s \to +\infty)$ at the appropriate minimum. An elementary argument[1] suffices to show that, apart from particle permutations, the expected number of distinct Φ minima rises exponentially with N in the large-N limit (fixed density).

Introduction of the mapping and of the resulting basins in the $3N$-dimensional configuration space effectively separates the statistical thermodynamics of the condensed phase into two parts. The first simply concerns the packing geometry of the particles, i.e., identification of the local Φ minima and classification of those minima by depth. The second involves evaluating the mean "vibrational" partition function for basins as a function of their depth. On account of this formal separation of packing from vibrational deformation, it becomes possible exactly (as $N \to +\infty$) to express the classical canonical partition function $Q_N(\beta)$, $\beta = (k_B T)^{-1}$, as a quadrature over $\phi \equiv \Phi/N$, the depth of minima on a per-particle basis[1]:

$$Q_N(\beta) = \lambda^{-3N} \int d\phi \exp\{N[\sigma(\phi) - \beta\phi - \beta f_v(\beta, \phi)]\}. \tag{1.2}$$

In this expression λ is the mean thermal deBroglie wavelength, $\exp[N\sigma(\phi)]$ is the distribution of distinguishable minima by depth, and f_v is the generally anharmonic vibrational free energy for basins of given depth

$$\exp[-N\beta f_v(\beta, \phi)] = \left\langle \int_{B_\alpha} dr \exp[-\beta \Delta_\alpha \Phi(\mathbf{r})] \right\rangle_\phi, \tag{1.3}$$

$$\Delta_\alpha \Phi(\mathbf{r}) = \Phi(\mathbf{r}) - \Phi(\mathbf{r}_\alpha).$$

Limits of integration for ϕ in Eq. (1.2) are set (a) at the lower end by the absolute Φ minimum corresponding to the best crystalline packing of particles, and (b) at the upper end by some form of "worst" packing. Between these limits the integrand will attain its maximum, say at $\phi_m(\beta)$, which is just the maximum of the exponent:

$$\sigma(\phi_m) - \beta\phi_m - \beta f_v(\beta, \phi_m) = \text{maximum}. \tag{1.4}$$

Because N is large the integral will be dominated by the contribution from the immediate neighborhood of this maximum, so that the free energy F for the system is given by

$$\beta F(\beta)/N = 3 \ln \lambda - \sigma(\phi_m) + \beta\phi_m + \beta f_v(\beta, \phi_m). \tag{1.5}$$

One of the surprising results that has emerged from this approach is that under constant density conditions, $\phi_m(\beta)$ is virtually constant over the entire temperature range of stability for the liquid phase, and can be accurately identified merely as the maximum of the packing entropy function σ.[3,5] This means that the liquid, regardless of its temperature, samples the dominating population of packings (they are amorphous) in the same *a priori* manner. Consequently there is a temperature-independent inherent structure underlying the liquid phase which is unveiled by the mapping to Φ minima.

Short-range order exhibited by the liquid can be examined by means of the correlation functions $g^{(2)}$, $g^{(3)}$, ..., the first of which is amenable to experimental measurement in real substances.[6] The short-range order present in the under-

 0021-9606/85/214767-09$02.10

lying inherent structure can be revealed by inspecting the corresponding set of "quench" correlation functions $g_q^{(2)}, g_q^{(3)},\ldots$. These latter are image-enhanced versions of the former, wherein vibrational deformation has been removed by the mapping to minima. More precisely, an ensemble of system configurations appropriate to some temperature generates $g^{(2)}, g^{(3)},\ldots$ for that temperature; the ensemble of images for those configurations after mapping generates $g_q^{(2)}, g_q^{(3)},\ldots$.

Numerical studies now exist of $g^{(2)}$ and $g_q^{(2)}$ for several different kinds of model liquids, including pure substances with different crystal structures,[3,7–9] binary mixtures,[10] and network formers with strongly nonadditive interactions.[11] In all cases the $g_q^{(2)}$'s are found to be independent of the temperature of the liquid prior to mapping. This is the short-range-order manifestation of the virtual temperature independence of $\phi_m(\beta)$ in the stable liquid phase. Temperature variations of the unquenched correlation functions $g^{(2)}, g^{(3)},\ldots$ evidently arise only from varying extents of vibrational deformation away from the potential minima.

Another benefit of the mapping and the associated basin construction is that the Lindemann melting criterion becomes reinterpreted and generalized.[12] In particular it is now possible to define rms return distances, for particles under the mapping, that have precise meaning both for the crystal phase and for the liquid phase. The former case leads to the Lindemann melting criterion for the crystal, the latter case leads to a new freezing criterion for the liquid.

The hard-sphere model historically has supplied a key element in the development of liquid-state theory.[13–16] Its intrinsic importance has been augmented by a variety of perturbation methods for both static[17–19] and kinetic[20] properties of liquids that utilize the hard-sphere model as an unperturbed reference system, and that then treat attractive forces between molecules as a weak perturbation. The guiding principle for these "van der Waals" theories of real liquids is that the hard cores almost exclusively determine the short-range order at a given density, and so the attractive longer-ranged forces primarily act to bind the dense liquid at the observed density.

The potential energy function $\Phi_{\rm HS}$ for the hard-sphere model is either zero or plus infinity, depending on whether or not all particle pair distances exceed the collision diameter a. On account of this singular behavior $\Phi_{\rm HS}$ has no discrete set of minima, and the mapping in Eq. (1.1) is not defined. Therefore it might appear superficially that the inherent structure approach to liquids has no insights to offer the hard-sphere model and its relatives, and vice versa.

However the two viewpoints can indeed be connected, and that is the objective of this paper. The hard-sphere pair interaction can be viewed as the limit of a sequence of functions that are smooth and bounded at positive separation. A particularly simple realization uses the inverse power functions:

$$\Phi_{\rm HS}(\mathbf{r}_1\ldots\mathbf{r}_N) = \lim_{n\to\infty} \sum_{i<j=1}^{N} (a/r_{ij})^n . \tag{1.6}$$

For any finite n, no matter how large, the mapping (1.1) is well defined; so too will the functions $\sigma, f_v, \phi_m g_q^{(2)},\ldots$ then be well defined. We will attempt to study the asymptotic behavior of the inherent structure theory for inverse power potentials as n becomes large.

The following Sec. II provides some general comments about inverse power potentials. Section III examines the asymptotic approach to the hard-sphere limit, and identifies the nature of the inherent structures that pertain to the hard-sphere limit. Section IV presents some molecular dynamics simulation results for two systems of 256 particles each, one with $n = 12$ and the other with $n = 24$, to supplement the purely analytical considerations. Section V contains some closing remarks.

II. INVERSE-POWER POTENTIALS

When the potential energy consists entirely of inverse-power central pair potentials,

$$\Phi(\mathbf{r}_1\ldots\mathbf{r}_N) = \sum_{i<j=i}^{N} (a/r_{ij})^n . \tag{2.1}$$

then in the large-system limit all excess intensive thermodynamic properties predicted by the classical partition function depend on number density ρ and inverse temperature β only through the single dimensionless variable[21]

$$\beta = \beta\rho^{n/3}a^n. \tag{2.2}$$

This simplification actually does not require pairwise interactions, but merely rises from the fact that Φ is homogeneous. Similarly, the correlation functions will be functions of reduced variables:

$$g^{(m)}(\mathbf{r}_1\ldots\mathbf{r}_n;\beta,\rho) = \bar{g}^{(m)}(\mathbf{r}_1/\rho^{1/3},\ldots,\mathbf{r}_n/\rho^{1/3};y). \tag{2.3}$$

The quantities σ and f_v which appear in the transformed partition function (1.2) likewise have simplified forms when interaction (2.1) applies. We can take them to be

$$\sigma(\phi,\rho) \equiv \bar{\sigma}(\rho^{-n/3}a^{-n}\phi), \tag{2.4}$$

$$\beta f_v(\beta,\phi,\rho) \equiv y\bar{f}(\rho^{-n/3}a^{-n}\phi, y). \tag{2.5}$$

As a result of these reductions, $\rho^{-n/3}a^{-n}\phi_m$ will be a function only of y.

The crystal structure of the thermodynamically stable solid phase depends on the value of n. Hoover, Young, and Grover[22] report that if $n > 7$ the low temperature crystal is face-centered cubic between absolute zero and the melting point; if $4 \leqslant n \leqslant 7$ they find that the stable crystal structure continues to be face-centered cubic at very low temperature, but undergoes a transition to body-centered cubic before the melting point is reached. We have carried out accurate lattice sums which show that the zero-temperature lattice energy remains minimized by the face-centered cubic structure for all $n > 3$.

Our subsequent considerations will be restricted to n values sufficiently large so that only the face-centered cubic crystal obtains at any temperature below the melting point.

For reference purposes, Fig. 1 shows plots of the pair potential $(a/r)^n$ for $n = 12,24,48,96$, and 192. Approach to the hard-sphere form is obvious in this sequence.

In the following we will suppose for convenience that

$$\rho a^3 \leqslant 1. \tag{2.6}$$

III. HARD-SPHERE LIMIT

The right member of the steepest descent Eq. (1.1) is $\mathbf{F}_j$, the net force on particle j due to all others:

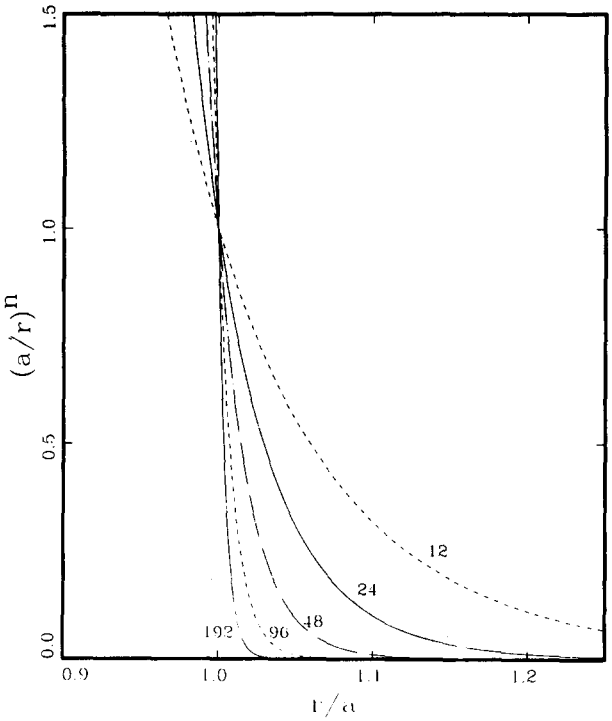

FIG. 1. Plots of inverse-power pair potentials $(a/r)^n$ for selected values of exponent n.

$$\mathbf{F}_j = \sum_{i(\neq j)} \mathbf{F}_{j,i}. \tag{3.1}$$

Here $\mathbf{F}_{j,i} = -\mathbf{F}_{i,j}$ is the force on j due to i. When Φ comprises inverse power pair potentials, we have

$$\mathbf{F}_{j,i} = (n/a)(a/\mathbf{r}_{ij})^{n+1}\mathbf{u}_{ij}, \tag{3.2}$$

where unit vector $\mathbf{u}_{ij}$ points from i to j:

$$\mathbf{u}_{ij} = (\mathbf{r}_j - \mathbf{r}_i)/\mathbf{r}_{ij}. \tag{3.3}$$

When n is very large the component forces $\mathbf{F}_{j,i}$ acting on particle j will be strongly ordered by magnitude, the largest corresponding to the smallest pair distance $\mathbf{r}_{ij}$, the next largest to the second smallest pair distance, and so on. This hierarchical ordering becomes ever more dramatic as n increases toward infinity, the hard-sphere limit.

The same situation applies to the full set of pair forces for the system as a whole. When n is very large, the particle pair with the smallest separation experiences a mutual repulsion that is orders of magnitude larger than that experienced by the pair with the next larger separation. This second pair in turn has a mutual force orders of magntiude larger than that of the third closest pair, etc. And again the discrepancy in magnitudes increases with n.

This hierarchical structure for large n has very clear implications for the steepest-descent mapping. At the beginning of the steepest descent ($s \gtrsim 0$), the closest particle pair, say ij, moves directly and symmetrically apart while over the same short time scale all other $N-2$ particles are substantially stationary. During this regime,

$$dr_{ij}/ds = (2n/a)(a/r_{ij})^{n+1}, \tag{3.4}$$

so that

$$r_{ij}(s) = [2n(n+2)a^n s + r_{ij}^{n+2}(0)]^{1/(n+2)}. \tag{3.5}$$

Eventually, at some positive "time" s_1, $\mathbf{r}_{ij}(s)$ will have increased to the point where it is virtually equal to the separation of that pair, say kl, which initially had the second smallest distance:

$$\mathbf{r}_{ij}(s_1) \cong \mathbf{r}_{kl}(0) \cong \mathbf{r}_{kl}(s_1). \tag{3.6}$$

At this stage the pair repulsions between ij and between kl have become comparable. Consequently, further increase in s has the two pairs moving apart at the same rate, while the remaining $N-4$ particles continue to be substantially stationary. Of course this assumes that ij and kl are totally distinct, which is certainly to be expected in a system of many particles.

Continuation of this process uncovers a sequence of times

$$0 < s_1 < s_2 < s_3 < \ldots \tag{3.7}$$

at which successively more and more particle pairs join the mutual distancing operation as they come into "contact," so to speak. Equation (3.4) describes the way that each such independent pair increases its separation with increasing s.

At some stage in this process it is to be expected that one of the separating pairs tu will encounter a nearby particle v, i.e.,

$$r_{tu}(s) = r_{uv}(s) \tag{3.8}$$

to form a contact-connected triplet. As Fig. 2 shows, subsequent motions of tuv dictated by the steepest descent Eqs.(1.1) cause the vertex angle at shared particle u to decrease until an equilateral triangle is formed, which then expands as such. Eventually triplets can grow to quadruplets or larger aggregates as more contacts come into play.

Quite obviously the process being described is entirely equivalent (as $n \to \infty$) to expansion of identical hard cores about every particle, coupled with motions of those particles away from one another when the cores come into contact so as just to avoid overlap. The contacts serve to partition the N particles into connected aggregates. Let $b(s)$ be the monotonically increasing effective hard core diameter at time s, and suppose for the given initial configuration of particles that the number of aggregates containing exactly j particles is $\mathbf{M}_j(s)$, where for all $s \geqslant 0$:

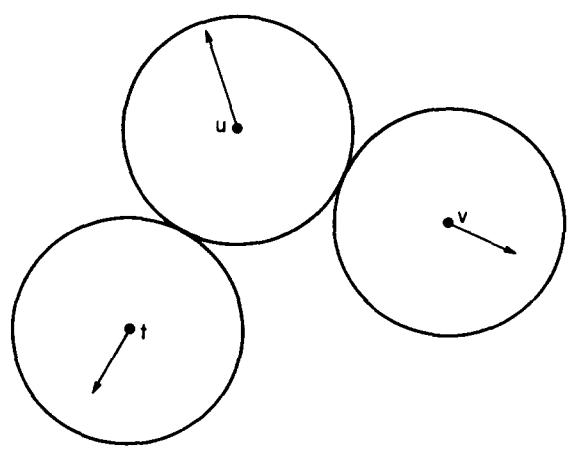

FIG. 2. Net forces (proportional to displacement rates) in a contact-connected triplet. Subsequent particle motions cause the vertex angle at u to decrease until an equilateral triangle forms.

$$N = \sum_{j=1}^{N} jM_j(s). \tag{3.9}$$

At $s = 0$, $\mathbf{M}_1 = N$ and all other $\mathbf{M}_j = 0$.

The process under consideration causes aggregates to grow, never to disconnect. Consequently, the mean aggregate size (reckoned on a per-particle basis)

$$N^{-1} \sum_{j=1}^{N} j^2 \mathbf{M}_j(s) \equiv A(s) \tag{3.10}$$

is nondecreasing, with

$$A(0) = 1. \tag{3.11}$$

Although $A(s)$ will be piecewise constant for any given initial configuration, its average over all initial conditions for a fixed system total energy is expected to be strictly monotonically increasing as a function of s, or of $b(s)$.

The particle aggregation by contact is a special kind of continuum percolation process,[23–25] and manifests a critical percolation threshold. This threshold is marked by that critical diameter b_c at which the mean aggregate size A switches over from order unity to order N. When $b(s) < b_c$ the clusters are essentially all small, and their normalized distribution is virtually independent of system size. However when $b_c < b(s)$ there will exist a system-spanning cluster that contains a nonvanishing fraction of all N particles. The critical percolation threshold is that point of the steepest-descent process at which global connectivity suddenly appears.

The existence of the percolation threshold requires that attention be given to the order of limits in which exponent n and particle number N separately approach infinity. If N were to go to infinity first, the growing aggregates at and above the percolation threshold may be too large (indeed infinite) to respond by translation or rotation to the demands of increasing b. That is, some fraction of the particles will no longer be able to increase their distance from neighbors any further, while at the same time others that are less completely impacted can continue to do so.

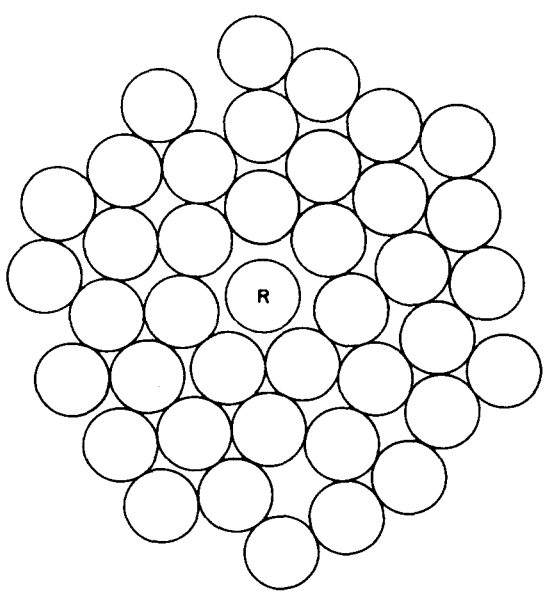

FIG. 3. Two-dimensional representation of a rattler (denoted by R) encased within a jammed configuration of hard cores. The cores by definition have diameter b_j.

To avoid this possible complication, we will suppose that for fixed N the exponent n passes first to infinity. Then subsequently we can ask what maybe the implications also of allowing N to become infinite at fixed number density ρ. With this convention on ordering of limits it becomes clear that b can increase through b_c without altering the basic process of uniformly expanding hard cores around all particle centers.

Eventually b reaches a value b_j at which the collection of particles becomes irremedially jammed. At this stage no local motion of the particles exists which would permit further b increase without occurrence of core overlap. Obviously, b_j depends on the initial configuration upon which the steepest-descent mapping operates. If that initial configuration had the N particles in a geometrically good approximation to one of the close-packed lattices (fcc, hcp, etc.), then jamming would occur when

$$\rho b_j^3 = 2^{1/2}. \tag{3.12}$$

On the other hand, a more disordered initial configuration such as might be encountered in the equilibrium liquid phase would almost certainly become jammed in a random packing, for which it is known[26] that

$$\rho b_j^3 \cong 1.22. \tag{3.13}$$

Jammed packings that are partly crystalline, partly amorphous could also occur with ρb_j^3 lying between values (3.12) and (3.13).

Not every one of the N particles need participate directly in the jamming. In principle there can be isolated "rattlers" trapped within a cage of particles which are themselves jammed, but all of which are further than b_j from the particle they enclose. Figure 3 provides a two-dimensional illustration. The concentration of these rattlers is likely to be quite small in both two- and three-dimensional cases. As the steepest-descent process continues beyond the jamming point, the predominating set of jammed particles will remain stationary, while the rattlers continue to displace to positions which locally maximize the minimum distance to their cage particles. When this is completed the endpoint of the steepest descent has been achieved.

Now we can let N approach infinity with ρ held fixed. We must then expect that the dispersion in b_j's resulting from various initial configurations for a given thermodynamic state, will vanish in that limit. In other words almost all steepest-descent mappings will jam at a common effective core diameter b^*. On account of restriction (2.6) and result (3.13) it is guaranteed that

$$b^* > a. \tag{3.14}$$

Remember that a is the *physical* hard core size generated in the potential energy by allowing n to go to infinity; b^* is the *effective* hard core size that establishes the jamming point for the collection of particles. Inequality (3.14) represents a kind of "core inflation."

We can now ask what these considerations imply for the quench pair correlation function $g_q^{(2)}(r)$. A trivial observation is that

$$g_q^{(2)}(r) = 0 \quad (0 \leqslant r \leqslant b^*). \tag{3.15}$$

More interesting is the behavior at $r = b^*$, where jamming causes each particle to touch an average number z of neigh-

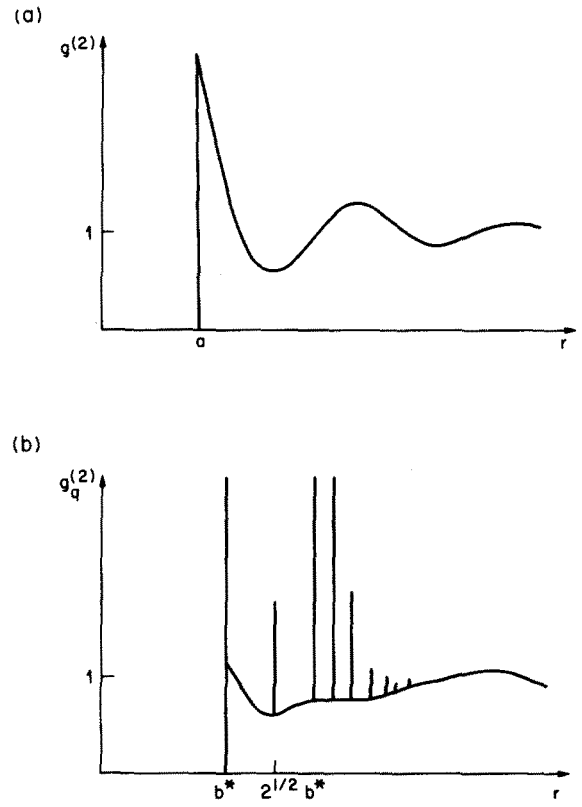

FIG. 4. Transformation (schematic) of the hard-sphere pair-correlation function by the steepest-descent mapping. Part (a) shows the conventional fluid-phase pair-correlation function; part (b) shows the quench pair-correlation function with Dirac delta-function contributions indicated as vertical line segments at appropriate distances.

bors. Under the assumption that the concentration of rattlers is negligible the mechanical condition of jamming in three dimensions requires

$$z \geqslant 4. \tag{3.16}$$

Since

$$\lim_{\epsilon \to 0} 4\pi\rho \int_{b^*-\epsilon}^{b^*+\epsilon} g_q^{(2)}(r) r^2 dr = z, \tag{3.17}$$

it is clear that $g_q^{(2)}$ must contain a Dirac delta-function contribution centered at b^*, specifically,

$$(z/4\pi\rho b^{*2})\delta(r - b^*). \tag{3.18}$$

For $r > b^*$, $g_q^{(2)}$ will contain a piecewise-continuous background part from pairs that had not managed to come into contact before jamming occurred.

It is natural to inquire whether Eq. (3.18) is the only delta-function contribution to be expected in $g_q^{(2)}$. The conclusion is that others must also appear. We expect to find distributed throughout even an amorphous random packing a nonvanishing concentration of fragments from the regular fcc and hcp lattices. This would produce a family of delta functions at the appropriate multiples of b^* with magnitudes that diminish rapidly with increasing distance. The first few of these multiples are[27]

$$b^*,\ 2^{1/2}b^*,\ (8/3)^{1/2}b^*,\ 3^{1/2}b^*,\ (11/3)^{1/2}b^*,\ 2b^*. \tag{3.19}$$

Whether fragments of other lattices (such as bcc) could also contribute delta functions is a question we shall leave open for the present.

That $g_q^{(2)}$ should be a highly singular function of r should come as no surprise, since the hard-sphere interaction itself is so obviously singular. In fact, the conventional pair correlation function $g^{(2)}$ for hard spheres apparently[28] is a nonanalytic function of r for all $r > a$.

Several investigations have been published concerning the properties of (jammed) random packings of hard spheres.[29–31] The binning methods that they typically have used for the pair correlations are not particularly well suited to detect the presence of Dirac delta functions beyond the hard core contact distance. Nevertheless, at least some of the results contain peaks that occur at some of the positions (3.19), and which may indeed indicate the presence of Dirac delta function contributions.

Figure 4 schematically shows how the steepest-descent mapping in the hard-sphere limit transforms the pair-correlation function. Part (a) represents the conventional $g^{(2)}(r)$, presumed to pertain to the fluid phase of the hard-sphere model (the transition densities are known to be $\rho a^3 = 0.943$ at the fluid's freezing point, $\rho a^3 = 1.040$ for the crystal's melting point.)[32] Part (b) represents $g_q^{(2)}(r)$ that results from the $n \to \infty$ limiting form of the configurational mapping.

IV. COMPUTER SIMULATIONS

While the analysis of the preceding section was directed at the infinite-n limit, it is also relevant for understanding the finite-n regime. Figure 1 provides a bit of guidance about how rapidly with n the hard-sphere limit is actually approached, but it does not really help in predicting the explicit n dependence of the pair correlation functions $g^{(2)}$ and $g_q^{(2)}$. For this latter feature we have turned to molecular dynamics computer simulation with frequent mapping to potential minima. Specifically, we have examined the cases $n = 12$ and 24.

The molecular dynamics calculations were carried out using a standard numerical procedure.[3,9] Both inverse-power choices were investigated using $N = 256$ particles subject to periodic boundary conditions. The primitive cell containing these particles was cubic with side length chosen so that

$$\rho a^3 = 0.818\,41 \tag{4.1}$$

(in fact we selected units for the computations for which $a = 1$). With either $n = 12$ or 24 the interactions are sufficiently short ranged so that a minimum-image convention for pair interactions can be (and was) used.

The integer 256 is appropriate for formation of the face-centered cubic crystal, free of defects and aligned with cubic box sides, with periodic images exactly in register with the particles at the box surfaces. This was the beginning configuration used for the molecular dynamics sequences for both n values.

Figure 5 shows the mean value $\langle \Phi \rangle$ of potential energy vs temperature for the case $n = 12$. The points shown correspond to a large collection of separately "equilibrated" states generated during a slow warming sequence. The data fall on two distinct branches, and indicate an upper bound to the true melting temperature at the given density due to the pos-

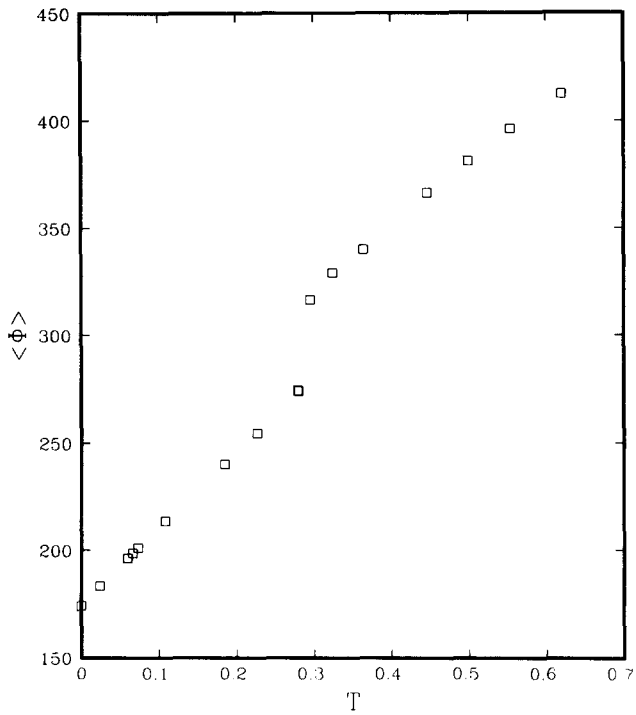

FIG. 5. Mean potential energy vs temperature for $n = 12$. The data shown pertain to molecular dynamics simulation for 256 particles at reduced density 0.818 41.

sibility of superheating:

$$T_m(n = 12) < 0.32. \tag{4.2}$$

In fact melting should occur[33] at reduced temperature 0.22.

Figure 6 shows the corresponding data, Φ vs temperature, for the more rigid potential $n = 24$. No doubt superheating again occurred, but a first-order melting nevertheless appears. Although no accurate determinations of $T_m(n = 24)$ have apparently ever been attempted, the trend suggested by known cases[33] indicates that it should only be about half of $T_m(n = 12)$. If indeed this is correct then we have produced even greater superheating for this second case, as might have been expected for such a steep potential with fixed-density conditions. Conclusions reached below are not affected by superheating.

The zero-temperature intercepts in Figs. 5 and 6 are the respective lattice sums for the perfect face-centered cubic crystals. For points of reference these have the values

$$\Phi(fcc) = 174.138\ 51\ (n = 12),$$
$$= 19.239\ 13\ \ (n = 24). \tag{4.3}$$

Of course this quantity converges to zero as n increases to infinity since the diameter-a hard spheres so generated would be out of contact [the nearest-neighbor separation in the fcc lattice is 1.2000 a at density (4.1)].

A pair of thermodynamic states in the stable fluid range was chosen for detailed study, one each for $n = 12$ and for $n = 24$. The respective temperatures were 0.3644 ($n = 12$) and 0.3149 ($n = 24$). Figures 7 and 8 provide the pair-correlation functions $g^{(2)}$ for each. That the first peak of the $n = 24$ $g^{(2)}$ is substantially higher than that for the $n = 12$ $g^{(2)}$ cannot be explained by the small temperature difference alone, but must be the result of shape change in the pair potential.

The $g^{(2)}$ curves in Figs. 7 and 8 and each represent averages over molecular dynamics runs of 10^4 steps of time increment $\Delta t = 5 \times 10^{-3}$ (particles have unit masses). Mapping to potential minima was numerically constructed every 200 time steps, requiring over 50 equally spaced mappings from

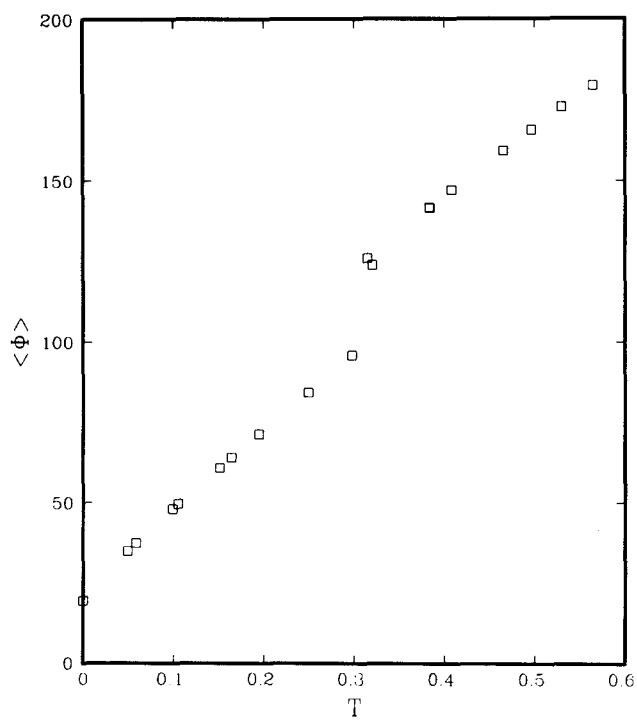

FIG. 6. Mean potential energy vs temperature for $n = 24$, via molecular dynamics simulation with 256 particles at reduced density 0.818 41.

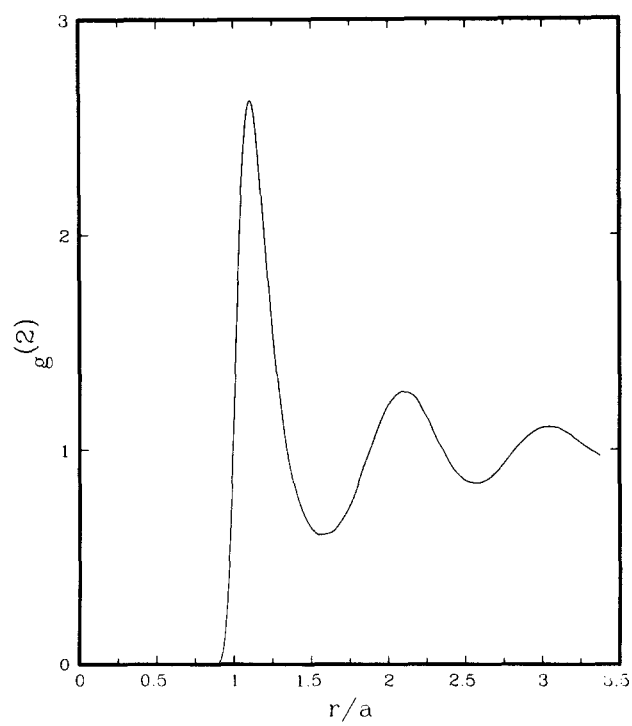

FIG. 7. Pair-correlation function $g^{(2)}(r)$ for the $n = 12$ system at temperature 0.3644. The density is 0.818 41.

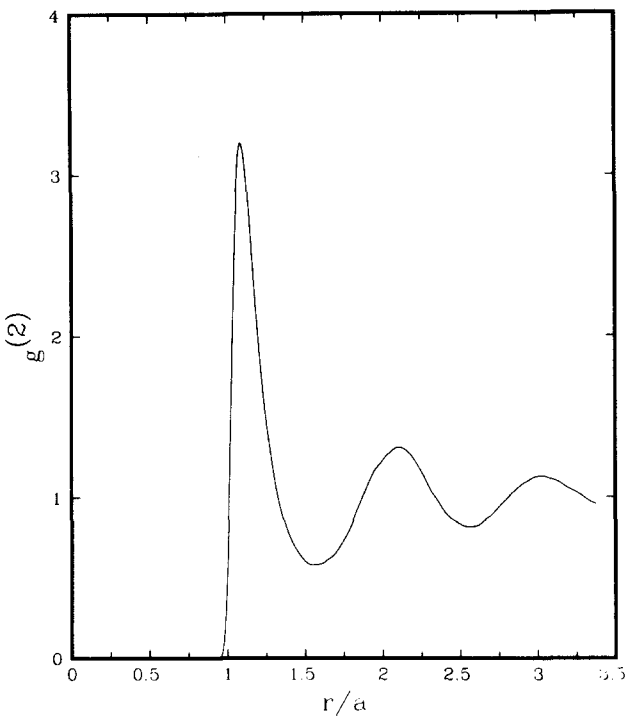

FIG. 8. Pair-correlation function $g^{(2)}(r)$ for the $n = 24$ system at temperature 0.3149. The density is 0.818 41.

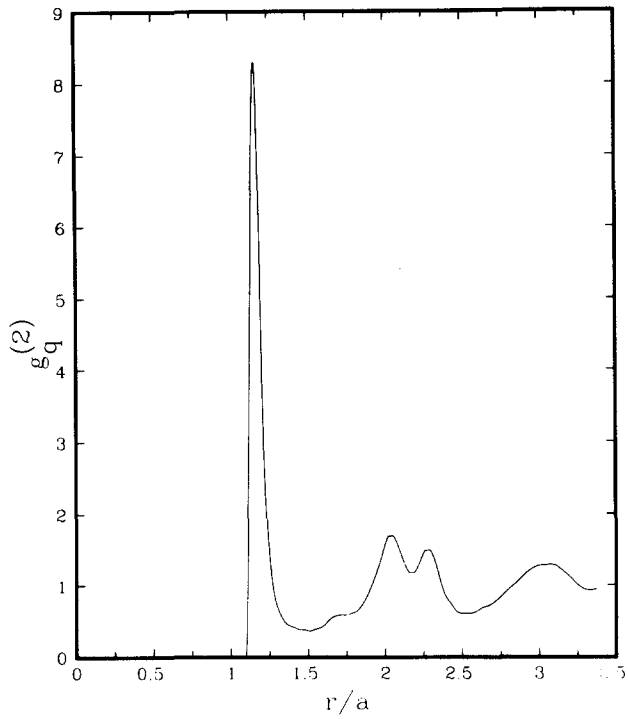

FIG. 10. Quench pair-correlation function $g_q^{(2)}$ for the $n = 24$ system at density 0.818 41 and prequench temperature 0.3149.

each of the two equilibrated fluid states. The resulting sets of Φ-minimum configurations then were used to calculate the corresponding $g_q^{(2)}$'s, shown in Figs. 9 and 10.

The transformation from $g^{(2)}$'s to $g_q^{(2)}$'s causes a dramatic enhancement of the image of short-range order. Not only is the first peak of each $g^{(2)}$ sharpened and heightened, but the initially featureless second peak is resolved into a split peak

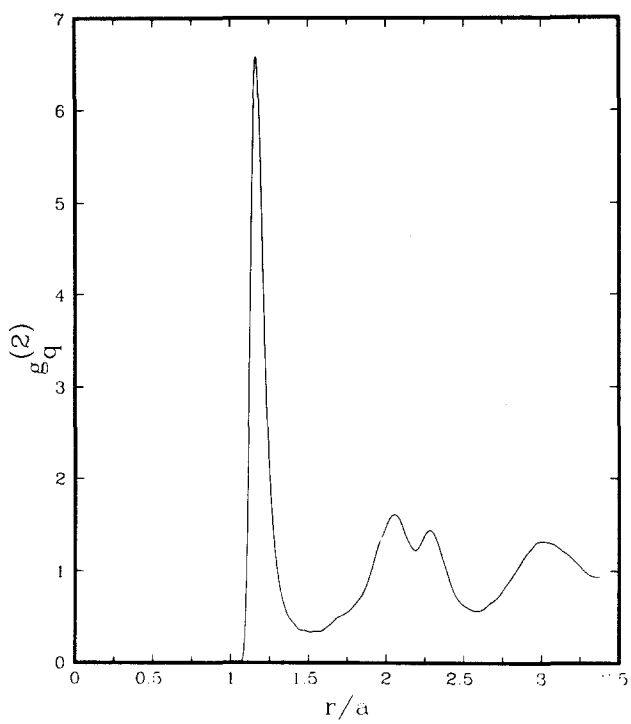

FIG. 9. Quench pair-correlation function $g_q^{(2)}$ for the $n = 12$ system at density 0.818 41 and prequench temperature 0.3644.

with a weak shoulder on the small-r side. Qualitatively, the $g_q^{(2)}$'s in Figs. 9 and 10 resemble not only one another, but they also closely resemble $g_q^{(2)}$'s that have previously been computed for other model fluids that likewise were known to crystallize in the face-centered cubic lattice.[8,34] The most reliable indicator of the form of $g_q^{(2)}$ for pure substances is in fact the equilibrium crystal structure that forms at the freezing point. For cases that form crystals distinct from face-centered cubic it has been established that $g_q^{(2)}$ has quite a different appearance.[9,34]

But beyond the superficial similarity between Figs. 9 and 10, careful examination reveals significant quantitative differences. Firstly, the value of $g_q^{(2)}$ at its first peak is 6.51 for $n = 12$, but rises to 8.17 for $n = 24$ (the respective peak positions are $r = 1.167$ and 1.165). Obviously this is the trend to be expected if, as $n \to +\infty$, the first peak is to narrow into a Dirac delta function an indicated above in Eq. (3.18). Secondly, the three components into which the mapping has resolved the second $g^{(2)}$ peak are considerably more distinctive for $n = 24$ than for $n = 12$. It is significant that these components occur close to $2^{1/2}$, $3^{1/2}$, and 2 times the distance of the first peak, strongly suggesting that local fragments of face-centered cubic lattices exist in these particle packings that also would sharpen to Dirac delta functions in the $n \to +\infty$ limit.

Figures 9 and 10 offer no evidence that the short-range order would totally sharpen into that of perfect close-packed arrays in the hard-sphere limit. The particle packings obtained from the fluid phase are manifestly amorphous, regardless of the n value.

Figures 11 and 12 present in graphical form the Φ values obtained numerically at the local minima, for each of the two cases. Comparison with Eq. (4.3) shows that every one of the

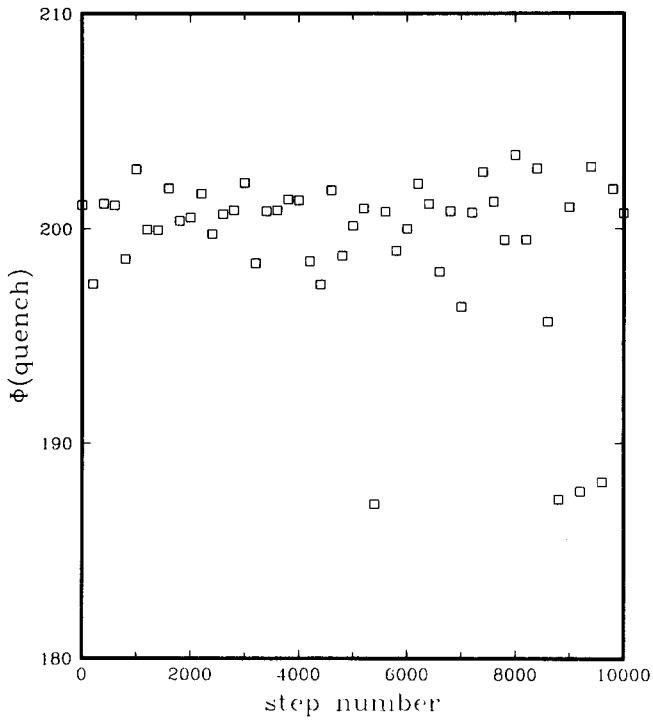

FIG. 11. Potential energy values at local minima obtained by quenching the $n = 12$ system from the fluid state at temperature 0.3644.

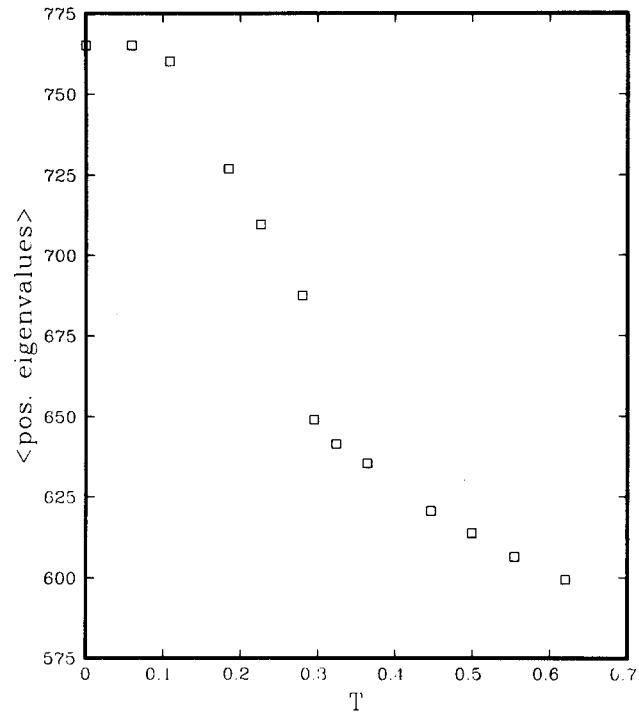

FIG. 13. Mean number of positive eigenvalues, vs temperature, for the $n = 12$ Hessian matrix.

mappings identified a local minimum lying above the absolute minimum. Both for $n = 12$ (Fig. 11) and for $n = 24$ (Fig. 12) the majority of the Φ values cluster closely together, however the distributions are both skewed to the low-Φ side. This latter feature had been identified previously as a characteristic of easily crystallizable models,[7] as distinct from glass formers.[10] The difference in Φ scales for these last two plots embody the collapse of all minima to the common value $\Phi = 0$ in the hard-sphere limit.

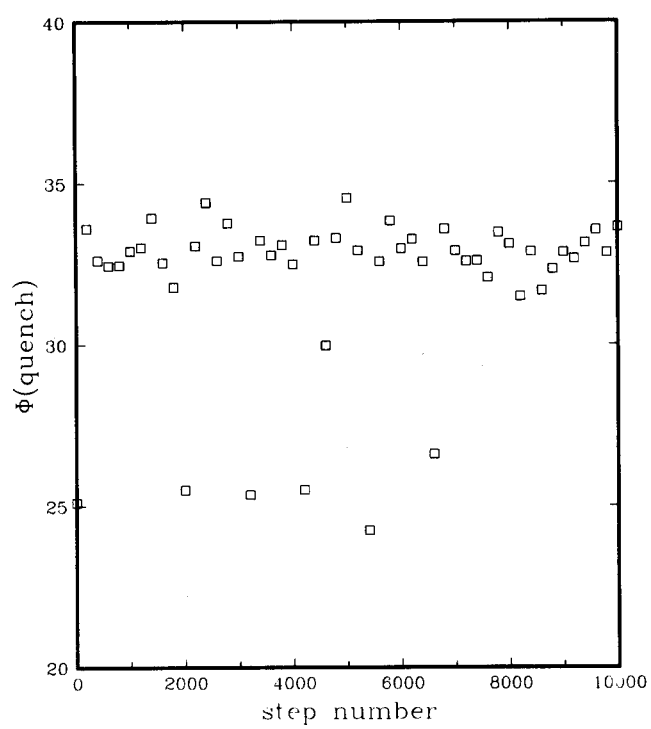

FIG. 12. Potential energy values at local minima obtained by quenching the $n = 24$ system from the fluid state at temperature 0.3149.

The Hessian matrix of second Φ derivatives, $\partial^2\Phi/\partial x_{i\alpha}\,\partial x_{j\beta}$, leads to a useful measure of anharmonicity.[34] If the dynamics confines the system to the immediate neighborhood of a potential energy minimum, then all eigenvalues (except for three corresponding to free center-of-mass motion) will be positive. However, if the dynamics entails large excursions from minima, the resulting anharmonicity would be expected to produce directions of downward curvature in Φ, i.e., some negative eigenvalues. In particular, passage across transition state regions would necessarily involve downward curvature.

Figures 13 (for $n = 12$) and 14 (for $n = 24$) show the mean number of positive eigenvalues for the Hessian matrix as a function of temperature. As expected, this is equal to 765 at low temperature, where the system executes very nearly pure harmonic motion about the absolute Φ minimum. But as temperature rises, a substantial proportion of the eigenvalues both for $n = 12$ and $n = 24$ tend to become negative, even before melting occurs. Furthermore, melting produces a discontinuous drop in the mean number of positive eigenvalues, indicating clearly that the fluid-phase portions of the Φ hypersurface are more anharmonic than the crystal-phase portions. Similar observations apply to a model for the noble gases, where both attractive and repulsive forces are present in the pair potential.[34]

V. DISCUSSION

The steepest-descent mapping and the particle packings it identifies are mathematically precise realizations of Bernal's intuitive ideas about short-range order in liquids.[35,36] As pointed out in the Introduction, these ideas have now been embedded in a statistical mechanical framework that shows

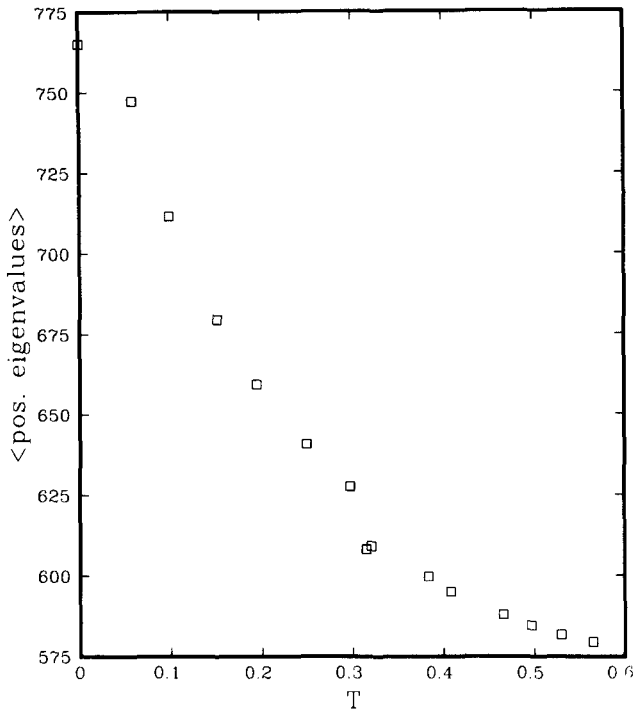

FIG. 14. Mean number of positive eigenvalues, vs temperature, for the $n = 24$ Hessian matrix.

their relevance to the canonical partition function and to the free energy. These connections emphasize the need to understand better the nature of particle packings.

To the extent that hard-sphere models will continue to provide a useful way to conceptualize condensed phases, it will be useful to investigate the nature of their amorphous packings. The approach followed in this paper indicates that computer construction of hard-sphere packings should probably not be carried out in the conventional manner in which particles are sequentially added on to a growing but otherwise immutable cluster.[30,37–40] Instead, it would be more relevant to start with an appropriate random distribution of points, continuously expand exclusion spheres about each, and move them apart as the steepest-descent procedure suggests, until finally jamming occurs.[41] This avoids the problems of anisotropy that inevitably plague the conventional packing construction approaches, and for the first time permits study of the interesting phenomenon of the rare rattlers. Furthermore, the exclusion-sphere expansion approach is easily adaptable to mixtures of spheres with different sizes (and even nonadditive radii), as well as to nonspherical shapes.

One of the more exciting developments in condensed matter chemical physics has been the identification of metastable binary alloys that exhibit icosahedral orientational order, but no translational order.[42] This creates a challenge to produce packings of two (or more) types of spheres which would have similar properties. We suspect it would be fruitful to adapt the exclusion-sphere expansion method to try to create such packings, in the hope that success would afford insight into the properties of real materials showing icosahedral order.

[1]F. H. Stillinger and T. A. Weber, Phys. Rev. A **25**, 978 (1982).
[2]F. H. Stillinger and T. A. Weber, J. Phys. Chem. **87**, 2833 (1983).
[3]F. H. Stillinger and T. A. Weber, Phys. Rev. A **28**, 2408 (1983).
[4]F. H. Stillinger and T. A. Weber, Science **225**, 983 (1984).
[5]F. H. Stillinger and T. A. Weber, J. Chem. Phys. **81**, 5095 (1984).
[6]T. L. Hill, *Statistical Mechanics* (McGraw–Hill, New York, 1956), Chap. 6.
[7]T. A. Weber and F. H. Stillinger, J. Chem. Phys. **80**, 2742 (1984).
[8]F. H. Stillinger and T. A. Weber, J. Chem. Phys. **80**, 4434 (1984).
[9]T. A. Weber and F. H. Stillinger, J. Chem. Phys. **81**, 5089 (1984).
[10]T. A. Weber and F. H. Stillinger, Phys. Rev. B **31**, 1954 (1985).
[11]F. H. Stillinger and T. A. Weber, Phys. Rev. B **31**, 5262 (1985).
[12]R. LaViolette and F. H. Stillinger, J. Chem. (to be published).
[13]J. G. Kirkwood, E. K. Maun, and B. J. Alder, J. Chem. Phys. **18**, 1040 (1950).
[14]W. W. Wood and J. D. Jacobson, J. Chem. Phys. **27**, 1207 (1957).
[15]B. J. Alder and T. E. Wainwright, J. Chem. Phys. **27**, 1208 (1957).
[16]H. Reiss, H. L. Frisch, and J. L. Lebowitz, J. Chem. Phys. **31**, 369 (1959).
[17]H. C. Longuet-Higgins and B. Widom, Mol. Phys. **8**, 549 (1964).
[18]D. Chandler, J. D. Weeks, and H. C. Andersen, Science **220**, 787 (1983).
[19]J. P. Hansen and I. R. McDonald, *Theory of Simple Liquids* (Academic, New York, 1976), Chap. 6.
[20]S. A. Rice and P. Gray, *The Statistical Mechanics of Simple Liquids* (Wiley–Interscience, New York, 1965), Chap. 5.
[21]W. G. Hoover and M. Ross, Contemp. Phys. **12**, 339 (1971).
[22]W. G. Hoover, D. A. Young, and R. Grover, J. Chem. Phys. **56**, 2207 (1972).
[23]J. W. Essam, in *Phase Transitions and Critical Phenomena*, edited by C. Domb and M. S. Green (Academic, New York, 1972), Vol. 2, pp. 197–270.
[24]F. H. Stillinger, J. Chem. Phys. **38**, 1486 (1963).
[25]F. H. Stillinger, Int. J. Quantum Chem. Quantum Chem. Symp. **16**, 137 (1982).
[26]L. V. Woodcock, Ann. N.Y. Acad. Sci. **371**, 274 (1981).
[27]J. O. Hirschfelder, C. J. Curtiss, and R. B. Bird, *Molecular Theory of Gases and Liquids* (Wiley, New York, 1954), pp. 1037–1039.
[28]F. H. Stillinger, J. Comput. Phys. **7**, 367 (1971).
[29]J. L. Finney, Proc. R. Soc. London A **319**, 479 (1970).
[30]C. H. Bennett, J. Appl. Phys. **43**, 2727 (1972).
[31]J. L. Finney, Nature **266**, 309 (1977).
[32]W. G. Hoover and F. H. Ree, J. Chem. Phys. **49**, 3609 (1968).
[33]Reference 19, p. 361.
[34]R. A. LaViolette and F. H. Stillinger (to be published).
[35]J. D. Bernal, Sci. Am. **203**, 125 (1960).
[36]J. D. Bernal, Proc. R. Soc. London Ser. A **280**, 299 (1964).
[37]D. J. Adams and A. J. Matheson, J. Chem. Phys. **56**, 1989 (1972).
[38]W. M. Visscher and M. Bolsterli, Nature **239**, 504 (1972).
[39]P. Mrafko and P. Duhaj, J. Non-Cryst. Solids **17**, 143 (1975).
[40]T. Ichikawa, Phys. Status. Solidi A **29**, 293 (1975).
[41]F. H. Stillinger, E. A. DiMarzio, and R. L. Kornegay, J. Chem. Phys. **40**, 1564 (1964).
[42]D. Shechtman, I. Blech, D. Gratias, and J. W. Cahn, Phys. Rev. Lett. **53**, 1951 (1984).